The Astrophysical Journal, 625:398–413, 2005 May 20

NUMERICAL MODELING OF DUSTY DEBRIS DISKS

A. T. Deller and S. T. Maddison
Centre for Astrophysics and Supercomputing, Swinburne University, P.O. Box 218, Hawthorn, VIC 3122, Australia
Received 2004 October 28; accepted 2005 February 2

ABSTRACT

Infrared and submillimeter observations of nearby Vega-like stars have revealed a number of clumpy, asymmetric dust debris disks. Previous studies using semianalytical and numerical methods have suggested planetary companions of various mass as the likely cause of most examples of disk asymmetry. In this paper, we modify an *N*-body symplectic gravitational integrator to include radiation terms and conduct medium-resolution parameter searches to identify likely planetary candidates in observed Vega-like systems. We also present high-resolution models of Vega and ϵ Eridani, comparing our results to those of previous authors, and a new model for Fomalhaut.

Subject headings: circumstellar matter — methods: *n*-body simulations — planetary systems — stars: individual (Vega, ϵ Eridani, Fomalhaut)

Online material: color figures

1. INTRODUCTION

Dust disks composed of particles in the micron to centimeter range are known to exist around many stars that exhibit an infrared excess, such as Vega, β Pictoris, and ϵ Eridani (see, e.g., Zuckerman 2001). Particles of this size are affected significantly by solar radiation and corpuscular (solar wind) forces, with Poynting-Robertson and solar wind drag resulting from the moving particle's absorption and reemission of solar energy. Over time, these dissipative forces caused by radiation and the solar wind act to reduce a dust particle's semimajor axis and eccentricity, and the particle eventually spirals into the central star (Burns et al. 1979). Since the age of most of these systems exceeds the expected lifetime of a small dust particle, the particles must be continually replenished. The suspected mechanism is a collisional cascade involving primordial planetesimal and smaller sized bodies (Backman & Paresce 1993; Wyatt & Dent 2002), as is believed to occur in the Edgeworth-Kuiper Belt (e.g., Backman et al. 1995; Landgraf et al. 2002). The destructive process that leads to dust formation has led these disks to be known as "debris disks."

Of the debris disks near enough to Earth to be spatially resolved, most show a significant degree of asymmetry (e.g., Vega: Holland et al. 1998; ϵ Eri: Greaves et al. 1998). The commonly held view is that gravitational interactions with an unseen embedded planet are responsible for most cases of disk structure (Ozernoy et al. 2000; Quillen & Thorndike 2002; Wilner et al. 2002). Alternative possible explanations have been considered for specific systems, such as disturbance by a passing star (e.g., HD 141569; Clampin et al. 2003), a recent large cometary/planetesimal collision (e.g., Fomalhaut; Wyatt & Dent 2002), and contamination by a background feature such as a distant galaxy (e.g., Vega; Wilner et al. 2002).

A planetary companion has several effects on an initially uniform debris disk. Particles near the planet are often ejected because of a close encounter, an effect that is enhanced as the planet's mass increases. Since particles interior to the planet spiral increasingly rapidly into the central star, an interior cleared zone is usually present (Liou & Zook 1999). However, some particles spiraling in toward the star may become trapped in a series of mean motion resonances (MMRs) with the planet. An MMR exists when the ratio of orbital periods for two objects orbiting a central mass is equal to $m:n$, where m and n are integers. The order of an MMR is given by the quantity $|m - n|$. The Earth has a dust ring formed by dust particles in MMRs (Dermott et al. 1994), and Neptune is suspected to do the same with Kuiper Belt dust (Liou & Zook 1999).

While locked into an MMR with a planet, the angular momentum of the particle lost to Poynting-Robertson and solar wind drag is balanced by the resonant forcing of the planet's gravitation. A particle trapped in an MMR can extend the particle's lifetime to many times the value predicted by Poynting-Robertson and solar wind drag alone. The resultant pileup of particles at discrete semimajor axes tends to cause prominent radial and angular structure in the debris disk (Kuchner & Holman 2003).

In multiple-planet systems, it is the outermost planet that generally dominates the structure of the resulting debris disk. Neptune is suspected to play this role in interactions with Kuiper Belt dust (Liou & Zook 1999). The interior planets, however, can have significant effects on particles that leak past the outermost planet. In the solar system, for example, Jupiter and Saturn eject many dust particles that drift interior to Neptune (Liou & Zook 1999). For simplicity, we investigate only single-planet systems and assume that the effects of any interior planets that may be present are negligible outside the orbit of the outermost planet.

In this paper, we numerically simulate a large number of debris disk systems, creating a synthetic debris disk catalog. Our numerical method is described in § 2, and the testing of the code is detailed in § 3. We present a small sample of the results from the synthetic catalog in § 4 and use the catalog to select planetary configurations that could be responsible for the observed systems of Vega, ϵ Eri, and Fomalhaut. The selected systems are then simulated in higher detail in § 5, and the results are compared to observational data. Our conclusions are presented in § 6.

2. NUMERICAL METHOD

We model the evolution of debris disks using an *N*-body integrator that includes the effects of radiation pressure and Poynting-Robertson and solar wind drag. In this section we discuss the modifications made to a symplectic integrator to account for the

additional forces, as well as our numerical techniques for creating debris disks and recording particle positions.

2.1. *The RMVS3 Integrator*

Since the general problem of a particle moving under the influence of gravitational and radiation forces is nonlinear, it is necessary to numerically integrate the orbits of all particles. Commonly used integrators include Runge-Kutta, Bulirsch-Stoer, and mixed variable symplectic (MVS) algorithms. The MVS integrator developed by Wisdom & Holman (1991) is normally the fastest, but it has the disadvantage of being unable to follow close encounters between particles and planets, which are crucial to debris disk evolution. This drawback has been overcome with the use of integrators such as RMVS3 (Levison & Duncan 1994) and SyMBA (Duncan et al. 1998), which are based on the Wisdom & Holman (1991) scheme but can integrate close encounters. In this work we have modified RMVS3 to include radiation and solar wind forces that affect debris disk particles. Such an approach was used by Moro-Martin & Malhotra (2002), who modify a variant of SyMBA. (Note that SyMBA and RMVS3 handle close encounters between particles and planets in different ways.)

RMVS3 assumes that test particles are both massless and collisionless; the problem of dust collisions is discussed in § 4.1. The code requires units such that the gravitational constant $G = 1$, and so we have chosen distance, time, and mass units to be 1 AU, 1 yr, and $M_\odot/(4\pi^2)$, respectively. Throughout this paper we use a for the semimajor axis, e for eccentricity, and i for inclination, with the subscripts "tp," "pb," and "pl" referring to a test particle, parent body, and planet, respectively.

As developed in Wisdom & Holman (1991) and described in Levison & Duncan (1994), RMVS3 expands the Hamiltonian of a test particle into two integrable components given by

$$H = H_{\rm Kep} + H_{\rm dist}, \tag{1}$$

where $H_{\rm Kep}$ represents the Keplerian motion around the central star and $H_{\rm dist}$ represents the perturbations on a test particle resulting from the planet(s). Using a time step Δt, the second-order approximation implemented in RMVS3 consists of applying the disturbance Hamiltonian for $\Delta t/2$, applying the Keplerian Hamiltonian for Δt, and then applying the disturbance Hamiltonian again for $\Delta t/2$. The approximation is accurate as long as the planetary disturbances are small compared to the Keplerian evolution. This assumption of small disturbances does not hold when a particle suffers a close encounter with a planet. In this situation, since the gravitational effect of the planet on the particle exceeds that of the star, the roles of planet and star are reversed and the Keplerian portion of the Hamiltonian is taken to occur around the planet and the star is relegated to the role of disturbance (Levison & Duncan 1994). Although a smaller time step is used during a close encounter, the duration of an encounter is typically small enough that the simulation proceeds rapidly. In the intermediate region in which planetary and stellar forces are comparable, the time step is also reduced but the integration remains heliocentric.

2.2. *Addition of Radiation and Solar Wind*

The magnitude of the radiation force on a particle is given by

$$\left|F_{\rm rad}\right| = \frac{LAQ_{\rm PR}}{4\pi c r^2}, \tag{2}$$

where L is the stellar luminosity, A is the particle cross-sectional area, $Q_{\rm PR}$ is the radiation pressure coefficient, c is the speed of light, and r is the heliocentric distance. It is standard practice to describe the strength of the radiation force on a given particle as a fraction of the gravitational force on a particle, such that

$$F_{\rm rad} = \beta F_{\rm grav}. \tag{3}$$

The constant β depends on the particle size and composition, as well as the stellar mass and luminosity, but is independent of the particle's heliocentric distance. The magnitude of Poynting-Robertson drag is proportional to β. The ratio of solar wind drag to Poynting-Robertson drag is dependent on particle size but is relatively constant over the range of particles usually considered ($s > 0.5$ μm; Burns et al. 1979), so the combined effects of Poynting-Robertson and solar wind drag can be expressed using a single parameter given by

$$\beta_{\rm sw} = \beta(1 + {\rm sw}), \tag{4}$$

where "sw" is the ratio of solar wind drag to Poynting-Robertson drag (Burns et al. 1979). Following Moro-Martin & Malhotra (2002), we use a constant value of sw = 0.35 in all our simulations.

The acceleration on a particle due to solar wind drag and radiation, ignoring terms of order $(v/c)^2$ and higher, is given by

$$\frac{d^2\boldsymbol{r}}{dt^2} = F_{\rm grav}\left[\beta\hat{\boldsymbol{r}} - \frac{\beta_{\rm sw}}{c}(v_r\hat{\boldsymbol{r}} + \boldsymbol{v})\right]. \tag{5}$$

The first term in this expression is the result of the outwardly directed radiation pressure, which causes the net acceleration in the radial direction to be reduced to $(1 - \beta)F_{\rm grav}$. The remaining two terms (which are smaller by a factor of v/c) represent the Poynting-Robertson and solar wind drag. Poynting-Robertson drag results from the particle's motion relative to the radiation source, which causes a component of the radiation force to oppose the particle's motion. During normal particle movement, the first term is accounted for in the Keplerian Hamiltonian by reducing the central object mass to the "apparent" value, whereas the other terms are added to the disturbance Hamiltonian. During a close encounter with a planet, the entire expression is added to the disturbance Hamiltonian.

2.3. *Particle Initialization*

All simulations commence with a central star, an orbiting planet, and a number of test particles distributed around the star with a fixed value of β. The star is fixed at the origin, and its mass is represented by M_*. The orbiting planet is described by $M_{\rm pl}$, $a_{\rm pl}$, and $e_{\rm pl}$, representing the planet's mass, semimajor axis, and eccentricity, respectively.

Test particles are assumed to be released from larger parent bodies (which are unaffected by radiation pressure) at the beginning of the simulation. This is analogous to the creation of dust through the collision of larger rocky bodies in a debris disk. The concept of a parent body is used only to set initial orbital parameters for test particles; they play no part in the simulation after initialization. For each simulation, the initial distribution of parent bodies is specified by a range of semimajor axis, eccentricity, and inclination values given by $a_{\rm pb}$, $e_{\rm pb}$, and $i_{\rm pb}$, respectively. The arguments of perihelion, longitudes of ascending nodes, and mean anomalies for the parent bodies are allocated randomly. A test particle is then created from each parent body, with semimajor axis, eccentricity, and inclination referred to by $a_{\rm tp}$, $e_{\rm tp}$, and $i_{\rm tp}$, respectively. Since the test particles are affected by radiation pressure while the parent bodies are not, the test particles have different orbital parameters from

their parent bodies. In particular, the test particles have increased semimajor axes and changed eccentricities, which are given by

$$a_{\rm tp} = a_{\rm pb}\frac{1-\beta}{1-2a_{\rm pb}\beta/r}, \tag{6}$$

$$e_{\rm tp} = \left[1 - \frac{\left(1-2a_{\rm pb}\beta/r\right)\left(1-e_{\rm pb}^2\right)}{(1-\beta)^2}\right]^{1/2}. \tag{7}$$

2.4. *Particle Recording*

Simulating a sufficient number of test particles to resolve the disk structure at all times is computationally expensive, and an alternative method used by Liou & Zook (1999) and Moro-Martin & Malhotra (2002) simulates a smaller number of particles and regularly records their positions, which can then be summed to produce distribution maps. A simulation is terminated after a fixed time or when all particles have been destroyed through either ejection via close encounters with planets or accretion onto the central star. In this way, long-lived particles (trapped in resonances) contribute more to the final dust distribution. If we assume the dust distribution is ergodic and that the total dust mass is constant (i.e., the dust production rate equals the loss rate), this approach should give an accurate representation of the actual "steady state" disk structure.

In previous studies (e.g., Moro-Martin & Malhotra 2002) the particle locations have been transformed into a reference frame that rotates with the outermost planet, but this approach is not appropriate for planets with eccentric orbits. For this reason, we instead ensure that the particle recording takes place with the planet in specific orbital phases. In this way a number of snapshots of the system are taken with the planet in varying locations, allowing the effect of planetary phase to be studied (Wilner et al. 2002; Kuchner & Holman 2003). For example, many simulations used a planet with orbital period 300 yr and a particle recording time of 1000 yr, resulting in particle distributions for three different planetary phases.

It should be noted that there are some limitations to this procedure of simulating a debris disk using a small number of test particles. As discussed by Moro-Martin & Malhotra (2002), because both the probability of being trapped in a particular resonance and the time spent in a resonance depend sensitively on initial conditions, using a limited number of particles may overexaggerate the importance of a particular resonance. We have tried to overcome this problem by using an order of magnitude more particles than previous authors (e.g., Quillen & Thorndike 2002; Moro-Martin & Malhotra 2002) in higher resolution simulations (see following sections). An additional problem with this procedure is that all the test particles are released from their parent body at the same time, with a specific planetary phase. In reality, dust particles would be released continuously at random planetary phases. This effect, however, is not likely to have a significant impact, since the test particles are typically released a long way from the planet and are distributed randomly around the star.

Setting a fixed maximum simulation time may also be problematic. For the small particle number approach to be accurate, the integration should be continued until all test particles have been destroyed. The termination of a simulation at a predetermined time means that some particles may still be active at the end of the simulation. One could argue, however, that extremely long-lived particles are unlikely to exist because of destruction via particle collisions. Since RMVS3 is a collisionless code, the destruction of particles in this way is not accounted for. We investigate these effects in more detail in § 4.1.

3. TEST CALCULATIONS

There is no general solution for the motion of a particle under the influence of radiation and gravitational forces in a system comprising a star and one or more planets. However, analytic solutions and analytic approximations exist for particle motion in the two-body (Wyatt & Whipple 1950) and the circularly restricted three-body (Liou & Zook 1997) problems, respectively. These specific cases can be used to check the accuracy of the modified RMVS3 code.

To ensure that the addition of radiation and solar wind forces did not affect the normal running of the code, we ran a series of tests in which β was set to zero and compared the results to identical tests run using the original RMVS3. The results were indistinguishable in all cases.

3.1. *The Two-Body Problem*

The time rate of change of a test particle's orbital elements in the radiation-modified two-body problem are given in Moro-Martin & Malhotra (2002) (following the work of Wyatt & Whipple [1950]; Burns et al. [1979]) and are equal to

$$\frac{da}{dt} = -\frac{(1+{\rm sw})\beta M_*}{c}\frac{(2+3e^2)}{a(1-e^2)^{3/2}}, \tag{8}$$

$$\frac{de}{dt} = -\frac{5(1+{\rm sw})\beta M_*}{2c}\frac{e}{a^2(1-e^2)^{1/2}}, \tag{9}$$

$$\frac{di}{dt} = 0, \tag{10}$$

where M_* is the mass of the central star and c is the speed of light.

To test the code against the two-body solutions, we ran a simulation with a single $\beta = 0.15$ test particle placed in orbit around a solar-mass star, released from a parent body with $a_{\rm pb} = 250$ AU, $e_{\rm pb} = 0.8$, and $i_{\rm pb} = 7.^\circ6$. The particle's argument of perihelion, longitude of ascending node, and mean anomaly were selected randomly. The analytical and numerical results plotted in Figure 1 are in excellent agreement.

3.2. *The Restricted Three-Body Problem*

The addition of a planet greatly complicates the motion of the test particle, but Liou & Zook (1997) have derived expressions for the time evolution of a particle's orbital elements while in an MMR with a zero-eccentricity planet. These expressions are a second-order approximation, valid only for low test particle eccentricities and inclinations and low-order resonances, and are given by

$$e^2 = \left[e_0^2 - (K-1)/3\right]\exp\left(3At/K\right) + (K-1)/3, \tag{11}$$

$$i = i_0\exp\left(-At/4\right), \tag{12}$$

where $A = (2\beta_{\rm sw}M_*)/(a^2c)$, $K = m/n$, e_0 and i_0 represent the particle's initial eccentricity and inclination, and m and n are the integers specifying the resonance. It should be noted that the location of resonances is shifted from their normal location because of the presence of the radiation force, which causes particles at a given semimajor axis to orbit more slowly because of

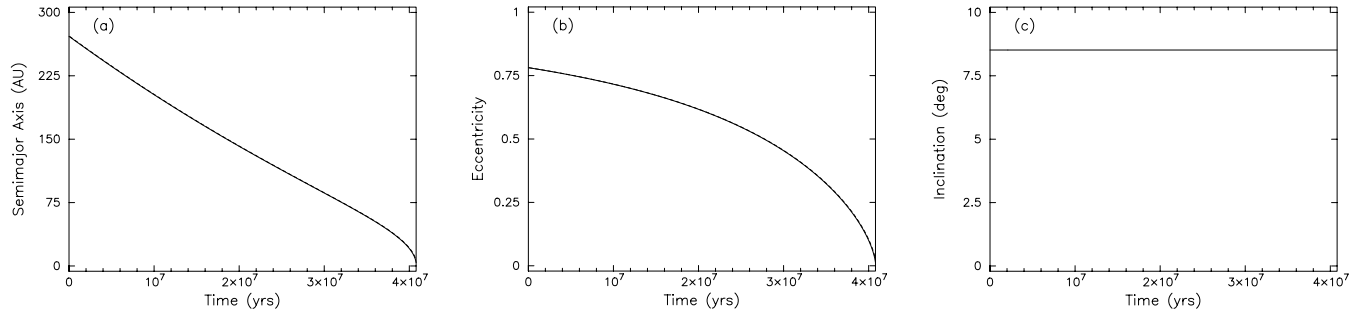

FIG. 1.—Time evolution of a single test particle orbiting a solar-mass star subject to Poynting-Robertson and solar wind drag. Plotted are the evolution of (*a*) $a_{\rm tp}$, (*b*) $e_{\rm tp}$, and (*c*) $i_{\rm tp}$ for a particle with $\beta = 0.15$ and sw $= 0.35$. The analytic solution (*dashed line*) and actual particle path (*solid line*) coincide.

the reduced effective gravitational force. The semimajor axis of a particle locked in an $m : n$ resonance with a planet is given by

$$a_{\rm tp} = a_{\rm pl}(1 - \beta)^{1/3}(m/n)^{2/3}. \quad (13)$$

We start at time $t = 0$ with a single particle placed exterior to the resonance in orbit around a 1 $M_\odot$ star and a planet at 30 AU. We follow the orbital evolution of the test particle as it passes through the MMR until it is ejected from the system and compare the results with equations (11) and (12).

We show the results for two different β-values. In Figure 2*a*, a single $\beta = 0.05$ particle is trapped in a 3:2 resonance with a Neptune-mass planet, whereas in Figure 2*b* a particle with $\beta = 0.2$ is trapped in a 2:1 resonance with a Jupiter-mass planet.

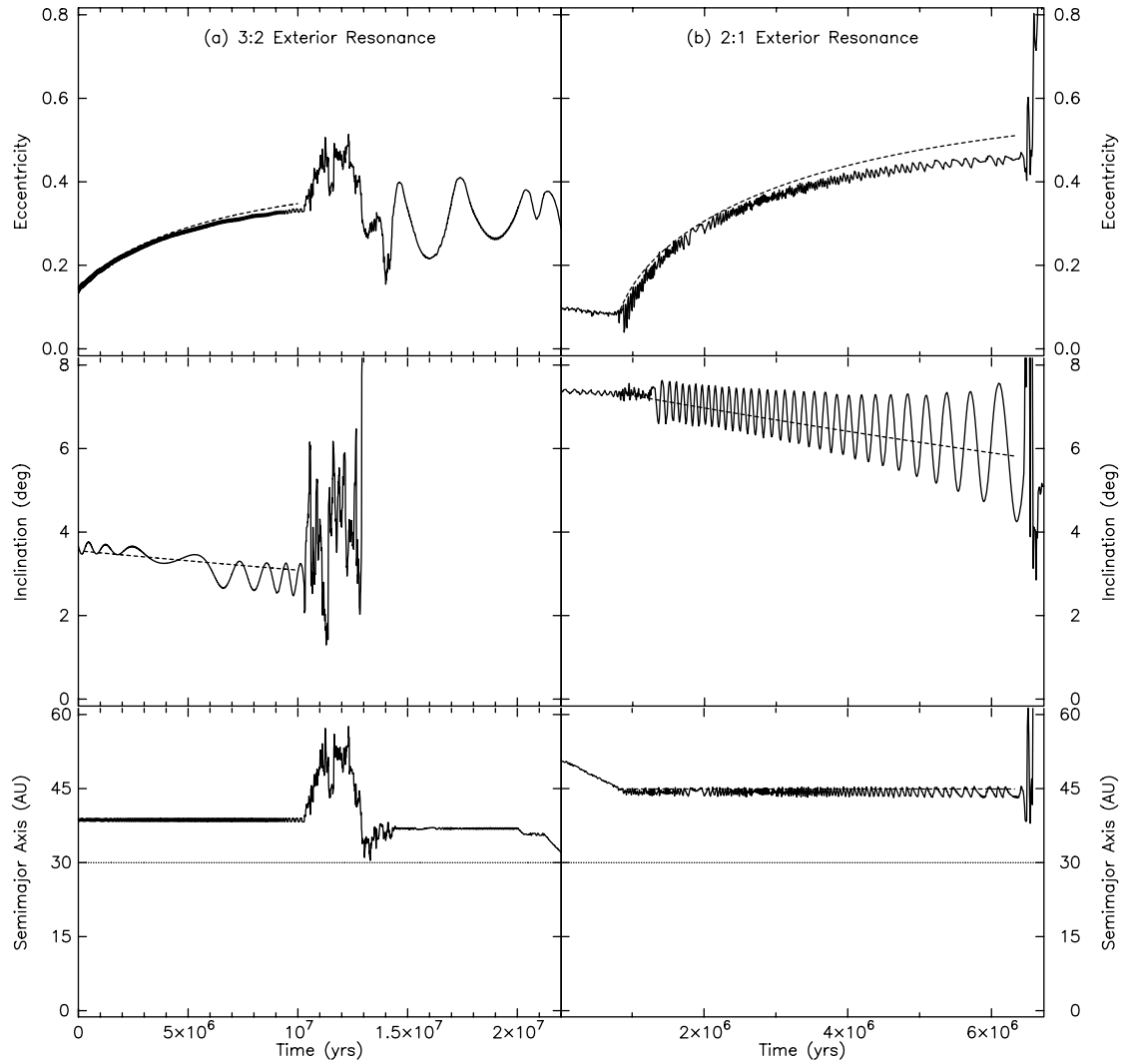

FIG. 2.—Evolution of a single test particle while in an MMR with a planet. The particle evolution is shown as a solid line, and the analytic solution is shown as a dashed line. The planetary semimajor axis is shown as a dotted line in the bottom two panels. (*a*) Particle with $\beta = 0.05$, in a 3:2 resonance with a $0.05M_{\rm J}$ planet. The particle is trapped for about 10^7 yr. (*b*) Particle with $\beta = 0.2$, in a 2:1 resonance with a Jupiter-mass planet. The particle is trapped for about 5 Myr. In both cases sw $= 0.35$.

TABLE 1
RANGE OF PARAMETER VALUES USED IN GENERATING OUR SYNTHETIC CATALOG

M_{pl}/M_J	e_{pl}	β	a_{pb}/a_{pl} [a_{min}, a_{max}]	e_{pb} [e_{min}, e_{max}]
0.01	0.0	0.01	[1.0, 1.4] (close)	[0.0, 0.2] (low)
0.05	0.1	0.1	[1.4, 2.0] (mid)	[0.1, 0.5] (medium)
0.2	0.3	0.2	[2.0, 3.5] (far)	...
1.0	0.5	0.4	...	...
3.0	0.7	...	...	...

NOTES.—Although this parameter space was not completely explored, approximately 300 of the 600 possible disks were simulated. Fully explored parameter subspaces (where the chosen parameter was simulated with all possible combinations of the other parameters) include $\beta = 0.1$, $M_{pl} = 0.05M_J$, and $M_{pl} = 1M_J$.

The particles' orbital elements are well described until their eccentricity and inclination become too large and the analytic solution becomes invalid. The results shown in Figure 2 are only a small sample of the large number of tests carried out to ensure the accuracy of the code.

4. A SYNTHETIC DEBRIS DISK CATALOG

Previous studies by Kuchner & Holman (2003) have predicted the general effects of varying planetary mass and eccentricity on the dust distribution in a debris disk. We have generated a synthetic catalog of debris disks that provides numerical agreement to the theoretical predictions and can be used as a guide when interpreting observed systems. Here we present a sample of results obtained from modeling over 300 disks, showing the effects of planetary mass and eccentricity, dust composition (β), and initial dust distribution on the disk structure. By generating simulated observations of these simulations, we show that even observations at a low resolution can distinguish between different planet and dust combinations.

For the creation of our synthetic catalog, we allowed five parameters to vary: M_{pl}, e_{pl}, β, a_{pb}, and e_{pb}. All other parameters were fixed as follows: $M_* = 1\ M_\odot$, $0^\circ < i_{pb} < 8^\circ$, $n_{tp} = 500$, and planetary period = 300 yr (yielding $a_{pl} \sim 44.8$ AU). Table 1 summarizes the parameter space we have investigated. Of the 600 possible combinations of our five free parameters, approximately 300 disks were simulated. Subsets of the parameter space that were fully explored include $\beta = 0.1$, $M_{pl} = 0.05M_J$, and $M_{pl} = 1M_J$.

Each simulation was run for 6×10^7 yr, corresponding to 2×10^5 planetary orbits. Particle positions were recorded every 1000 yr, allowing observation of the system in three different planetary phases. The maximum and minimum allowable heliocentric radii of the test particles were 700 and 2 AU, respectively.

At the end of each simulation, the recorded particle positions (in the three orbital phases) were binned in the *XY*-plane. The particle distribution in the *XY*-plane was then plotted for each particular planetary phase. We also binned particle semimajor axes and plotted the semimajor axis occupancy versus semimajor axis, which shows the location and strength of MMRs with the planet.

In order to produce synthetic observations of the systems, the particle distribution plots were weighted by estimated total disk mass and the dust emissivity at 850 μm, assuming the dust to be a perfect blackbody. This emissivity plot was then convolved with a two-dimensional Gaussian with a FWHM of 40 AU to simulate observations of the system with limited resolution. The synthetic observations can also be plotted from various disk viewing angles. This procedure assumes that the disk is optically thin, which is a reasonable assumption for disks containing little to no gas, as is the case for most Vega-like systems (Liseau 1999).

The complete synthetic catalog is available for viewing online.[1] Here we present a sample of results from our catalog for Jupiter- and Neptune-mass planets with $e_{pl} = 0.1$ and 0.5 in Figures 3 and 4. These simulations use $\beta = 0.1$ and test particles released from parent bodies with orbital elements $0 < e_{pb} < 0.2$, $1.4 < a_{pb}/a_{pl} < 2.0$, and $0^\circ < i_{pb} < 8^\circ$.

As can be seen in Figures 3 and 4, the mass and eccentricity of a planet dramatically alters the resulting dust distribution. The Jupiter-mass planet clears a central cavity, which is not as pronounced in the Neptune-mass case. In the low planetary eccentricity case, a relatively smooth dust ring is present external to the planet. When the planetary eccentricity is increased, the smooth ring vanishes, replaced by prominent arcs or clumps of dust emission. Similar trends were observed in the synthetic catalog with planets of different masses. These results closely resemble the predictions made by Kuchner & Holman (2003) for the four cases of (1) low-mass, low-eccentricity planets, (2) low-mass, moderate-eccentricity planets, (3) high-mass, low-eccentricity planets, and (4) high-mass, moderate-eccentricity planets.

Figure 5 shows the resonance occupations for the $e_{pl} = 0.1$ cases. The effect of planetary mass is again highlighted, with a high-mass planet trapping particles in a few strong resonances, mostly at higher semimajor axes, whereas a low-mass planet has many weaker resonances closer to the planet's semimajor axis. More accurate simulated observations for specific systems and telescopes are undertaken in § 5.

4.1. *Dust Lifetime and Collisional Processes*

As discussed in § 2.4, our numerical procedure of using a small number of particles can lead to potential problems when terminating the simulation at a specified time, since some long-lived particles may still be active. In a real debris disk, however, grain collisions would limit the maximum lifetime of particles.

In Figure 6 we show the results of a simulation of a Jupiter-mass planet with $a_{pl} \sim 44.8$ AU and $e_{pl} = 0.5$ system containing 500 test particles with $\beta = 0.1$. The test particles are released from parent bodies with $1.4 < a_{pb}/a_{pl} < 2.0$, $0.0 < e_{pb} < 0.2$, and $0\overset{\circ}{.}0 < i_{pb} < 8\overset{\circ}{.}0$. The three panels show the dust distribution when the simulation is terminated after 11.7, 40, and 153 Myr, corresponding to 10%, 2%, and 0% of particles remaining active, respectively. It can be seen that the basic disk structure is created rapidly, and the final few particles have a limited impact despite having lifetimes many times the median. The longest-lived particles tend to sharpen the distribution and bring out finer detail, which is hidden in our simulated observations (telescope FWHM of 40 AU). Thus, the imposition of a cutoff lifetime (whether as a numerical convenience or as a substitute for dust destruction through collisions) is of little consequence as long as most (>90%) particles have already been accreted or ejected.

5. MODELING OBSERVED SYSTEMS

In this section we use the synthetic disk catalog to select planetary configurations that generate structures similar to the observed debris disk systems Vega, ϵ Eri, and Fomalhaut. We

[1] See http://astronomy.swin.edu.au/debrisdisks.

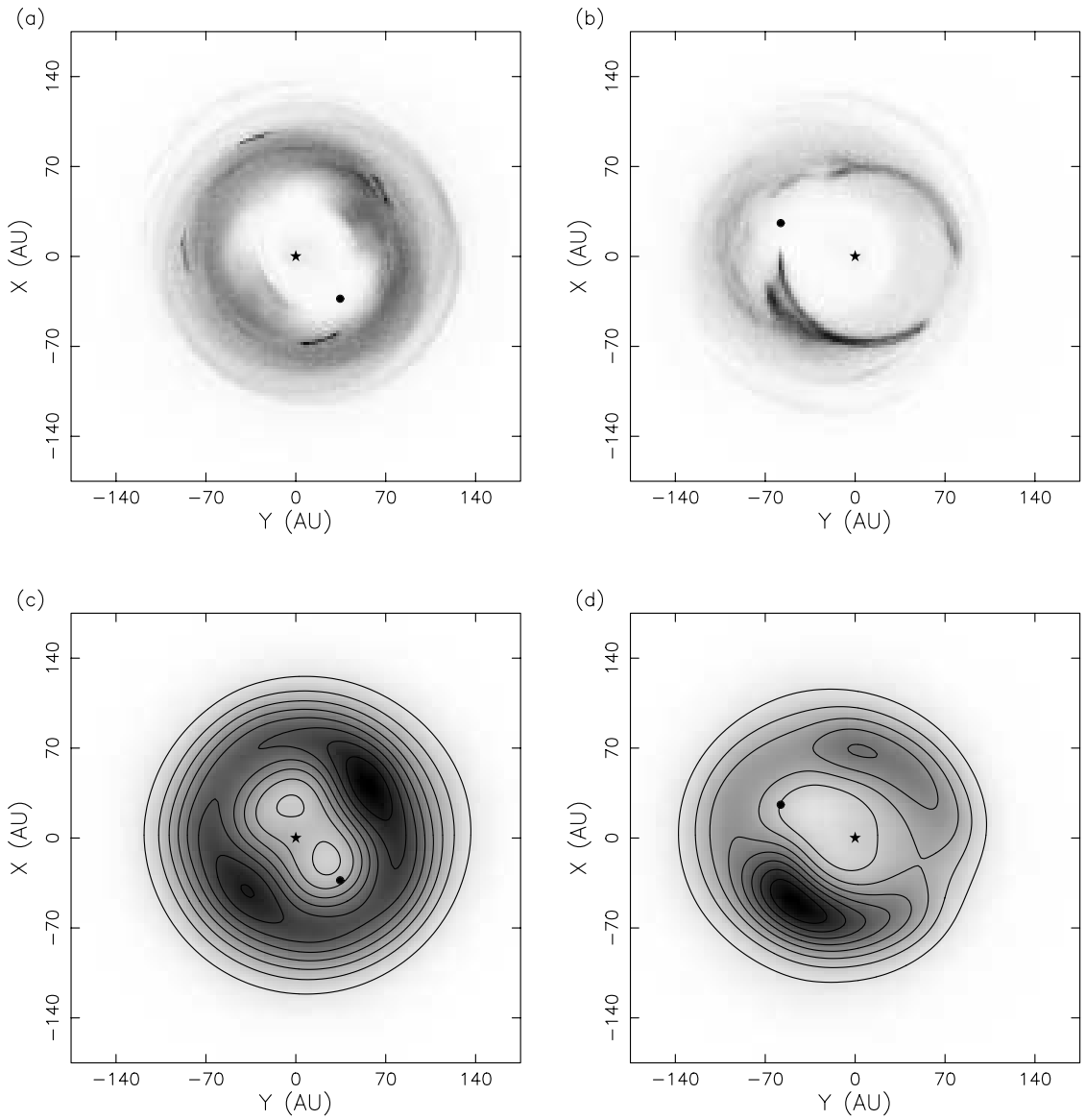

FIG. 3.—Simulations of a system containing a single Jupiter-mass planet and 500 test particles after 6×10^7 yr, or 20,000 orbital periods. In each case, the planet is located at $a_{\rm pl} \sim 44.8$ AU, and test particles were released from parent bodies with $1.4 < a_{\rm pb}/a_{\rm pl} < 2.0$, $0 < e_{\rm pb} < 0.2$, $0^\circ < i_{\rm pb} < 8^\circ$, and $\beta = 0.1$. The star and planet are represented by a filled star and circle, respectively. Plots (*a*) and (*b*) show the dust distributions generated when $e_{\rm pl} = 0.1$ and 0.5, respectively. Plots (*c*) and (*d*) show simulated observations of the disks (with beam FWHM of 40 AU) for $e_{\rm pl} = 0.1$ and 0.5, respectively. [*See the electronic edition of the Journal for a color version of this figure*.]

then optimize the planetary and parent-body parameters and increase the resolution (by increasing the number of test particles) to produce more accurate synthetic observations, which we compare to previous observational and numerical studies of these three debris disk systems.

5.1. *Vega*

Vega (α Lyr) was the first star identified with an infrared excess associated with a disk of dusty material (Aumann et al. 1984) and has become the prototype for so-called Vega-type stars. Subsequent observations with SCUBA (Holland et al. 1998) and the IRAM Plateau de Bure Interferometer (Wilner et al. 2002) confirm that Vega is surrounded by a dusty disk, with two prominent clumps of emission. Wilner et al. (2002) proposed that the twin lobes of emission seen in these images are caused by dust trapped in MMRs with a massive, eccentric planet ($M_{\rm pl} = 3M_{\rm J}$, $e_{\rm pl} = 0.6$) orbiting Vega with a semimajor axis of 40 AU. In their model, the initial test particle longitudes of perihelion were constrained to be aligned closely with the planet's longitude of perihelion (which is reasonable for a high-eccentricity system). They also noted that a wide variety of planetary parameters can produce the twin-lobed structure seen in Vega.

Although our code was able to reproduce the results of Wilner et al. (2002), their synthetic observations (at the resolution of the Holland et al. [1998] Vega observations) show nearly symmetrical emission, whereas the Holland et al. (1998) observations show a significant asymmetry. (It should be noted, however, that there are uncertainties in the Holland et al. (1998) observations. In the model we are about to present, we are assuming that the observed asymmetry is real.) On the basis of results from our synthetic catalog, we have modeled Vega using an entirely different planetary configuration in an attempt to better match these observations. In our model, a more distant ($a_{\rm pl} = 73.7$ AU), less eccentric ($e_{\rm pl} = 0.1$) $3M_{\rm J}$ planet reproduces the observed disk structure, with no constraints on the initial

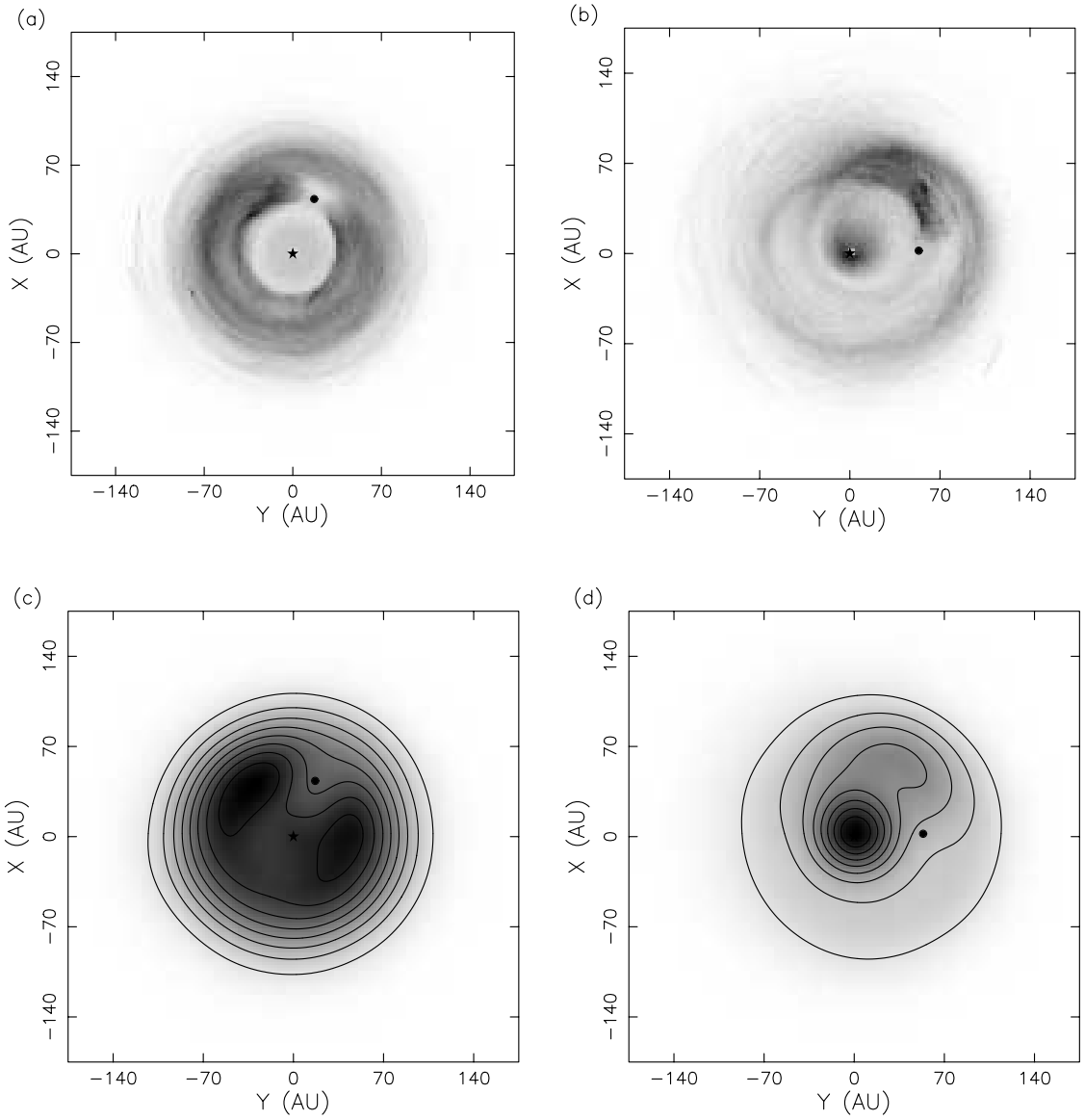

FIG. 4.—Simulations of a system containing a single Neptune-mass planet and 500 test particles after 6×10^7 yr, or 20,000 orbital periods. In each case, the planet is located at $a_{\rm pl} \sim 44.8$ AU, and test particles were released from parent bodies with $1.4 < a_{\rm pb}/a_{\rm pl} < 2.0$, $0 < e_{\rm pb} < 0.2$, $0^\circ < i_{\rm pb} < 8^\circ$, and $\beta = 0.1$. Plots (*a*) and (*b*) show the dust distributions generated when $e_{\rm pl} = 0.1$ and 0.5, respectively. Plots (*c*) and (*d*) show simulated observations of the disks (with beam FWHM of 40 AU) for $e_{\rm pl} = 0.1$ and 0.5, respectively. [*See the electronic edition of the Journal for a color version of this figure.*]

test particle perihelia (since we are modeling a lower eccentricity planet). We use 5000 test particles released from parent bodies with initial orbital elements in the ranges 90 AU $< a_{\rm pb} <$ 120 AU, $0.0 < e_{\rm pb} < 0.3$, and $0^\circ < i_{\rm pb} < 8^\circ$.

Dent et al. (2000) state that to fit the observed spectral energy distribution, the dust grains that make up the Vega disk must have diameters in the range 60–400 μm, corresponding to $\beta = 0.02-0.11$ for Vega's estimated mass and luminosity. We have simulated this system with β-values of 0.02, 0.05, and 0.1 and found negligible differences between the synthetic observations. (Note that Wilner et al. [2002] used $\beta = 0.01$ with sw = 0.) Figure 7 shows the dust distribution, simulated observation, and resonance occupancy plots obtained using our Vega model with $\beta = 0.05$.

We note that our model for Vega produces a dust distribution that is essentially stationary in the planet's frame of reference. Such a distribution means that as the planet orbits the star, observations from Earth will show positional changes in the emission peaks over an orbital timescale. Dust distributions from the four orbital phases recorded are shown in Figure 8.

The model accurately reproduces the twin lobes seen in the Wilner et al. (2002) observations, as well as the extended emission seen in the lower resolution Holland et al. (1998) observations. Figure 7*a* shows asymmetry in the two emission features, which are neither collinear with the star nor the same distance from the star, as seen in the Wilner et al. (2002) observations. This model also provides reasonable constraints on the orbital parameters of the proposed planet; for example, the same model with $e_{\rm pl} = 0.2$ results in a markedly different structure, as does a significantly less massive ($M_{\rm pl} < M_{\rm J}$) planet. The primary concern with this model is the requirement that such a massive planet have formed or migrated to such a large distance from the central star, although the fact that Vega is estimated to be 2.5 times as massive as the Sun may mitigate this problem. Future detailed observations are required to test our planetary model.

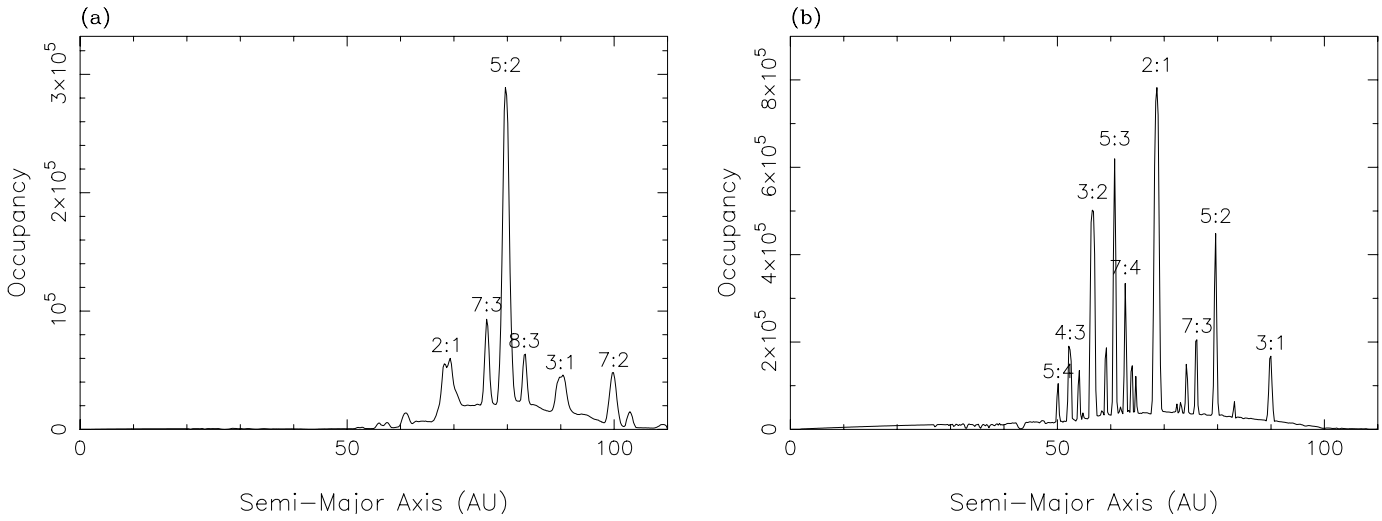

FIG. 5.—Resonance occupation for a system containing a single planet with (*a*) $M_{\rm pl} = M_{\rm J}$, (*b*) $M_{\rm pl} = 0.05 M_{\rm J}$. In each case, the planet has $e_{\rm pl} = 0.1$ and $a_{\rm pl} \sim 44.8$ AU. Note that the lower mass planet tends to trap particles in narrower resonances, closer to the planet's semimajor axis.

5.2. ϵ *Eridani*

First identified as a Vega-type star in 1984 (Aumann 1985), ϵ Eri has been the subject of ongoing planetary speculation since disk images taken at 850 μm by Greaves et al. (1998) showed a clumpy, asymmetric ring, with a cleared region interior to $\sim$30 AU. Radial velocity observations by Hatzes et al. (2000) detected a $1.7 M_{\rm J}$ planetary companion with $a_{\rm pl} \sim 3.4$ AU and $e_{\rm pl} \sim 0.6$. Such a close companion, however, cannot account for the observed disk structure seen by Greaves et al.

Numerical simulations by Ozernoy et al. (2000) have suggested the presence of a $M_{\rm pl} = 0.2 M_{\rm J}$, $a_{\rm pl} = 55$–65 AU, $e_{\rm pl} = 0.0$ planet, whereas Quillen & Thorndike (2002) proposed a $M_{\rm pl} = 0.1 M_{\rm J}$, $a_{\rm pl} = 41.6$ AU, $e_{\rm pl} = 0.3$ planet in the ϵ Eri disk. A planet with mass equal to or greater than that of Jupiter is unlikely to be responsible for the observed disk structure, since massive planets tend to trap particles in the n:1 resonances (Kuchner & Holman 2003). Our simulations of a Jupiter-mass planet, shown in Figure 9*a*, demonstrate this effect. For particles to occupy the $n + 1 : n$ resonances near a massive planet, their parent bodies must also reside very close to the planet, and in this situation most particles are quickly scattered or leak past the planet, as shown in Figure 9*b*. This results in a structure that lacks the observed central cavity of ϵ Eri (see Figs. 9*c* and 9*d*). The presence of the observed central clearing would then require the gravitational influence of a second, more massive planet at an intermediate semimajor axis (Liou & Zook 1999).

Ozernoy et al. (2000) consider only particles in the 2:1 and 3:2 resonances (in equal proportions), whereas Quillen & Thorndike consider only particles with $a_{\rm tp} = [1.1, 1.5] a_{\rm pl}$. An examination of our results shows why: if particles with semimajor axes smaller than the semimajor axis of the planet are allowed (as in Fig. 10*a*), emission from particles close to the star dominates and a ring structure is not seen (see Fig. 10*b*). The implied ejection of particles from the inner regions of the disk hints at another undiscovered and more massive planet at an intermediate distance from the star. The requirements for such a planet are discussed below.

We suggest that the system proposed by Ozernoy et al. (2000) is unlikely to be responsible for the ϵ Eri disk for two reasons: (1) their model is symmetrical, whereas the original observations by Greaves et al. (1998) and subsequent 350 μm observations by D. J. Wilner (2004, private communication) state that only the most prominent clump (in the southeast of the image) is definitely present, and (2) our simulations show that dust released in a range encompassing the 2:1 and 3:2 resonances will always occupy other resonances such as the 5:3 and that the resonance occupancies are rarely in equal proportion. We therefore investigate the model proposed by Quillen & Thorndike (2002) in more detail.

Our models differ somewhat from those of Quillen & Thorndike (2002) in that we use 5000 test particles (increasing the resolution by an order of magnitude), we include solar wind drag, and we model the system in three dimensions. The simulations were terminated after 3×10^8 yr, when less than 1% of the test particles remained active. Because the dominant grain size in the ϵ Eri disk has not been well determined, we have simulated the system using two β-values, $\beta = 0.1$ and 0.01. Initial parent body semimajor axes and eccentricities are set in the range $[1.1,\ 1.5] a_{\rm pl}$ and [0, 0.4], respectively, whereas initial inclinations are in the range $[0^\circ, 8^\circ]$. Our results are shown in Figure 10.

Both the $\beta = 0.1$ and $\beta = 0.01$ models reproduce the ring structure seen in the submillimeter observations, possessing a single prominent emission maximum and one or more secondary maxima. As expected, the contrast and detail is higher in the $\beta = 0.01$ case, since more particles are trapped in resonances for longer. Unlike Vega, this dust distribution generated by this model is not fixed in the planet's reference frame, but the emission peaks do show positional changes over a planetary orbit, as shown in Figure 11. Our results confirm the model proposed by Quillen & Thorndike (2002) as a viable explanation for the ϵ Eri system, with the caveat that an additional massive body must exist interior to the dust-sculpting planet's orbit.

In order to confirm that an inner planet is responsible for clearing the inner regions of the disk, one would like to simply introduce a second planet into the ϵ Eri model. However, since the introduction of a second planet introduces variations into the orbital elements of the primary outer planet, recording particle positions with the outer planet in an fixed position over time is no longer possible. We can instead introduce an inner planet to our model at a range of semimajor axes and use test particle occupancy versus semimajor axis plots to determine whether the inner planet effectively removes particles from the inner $\sim$40 AU of the system.

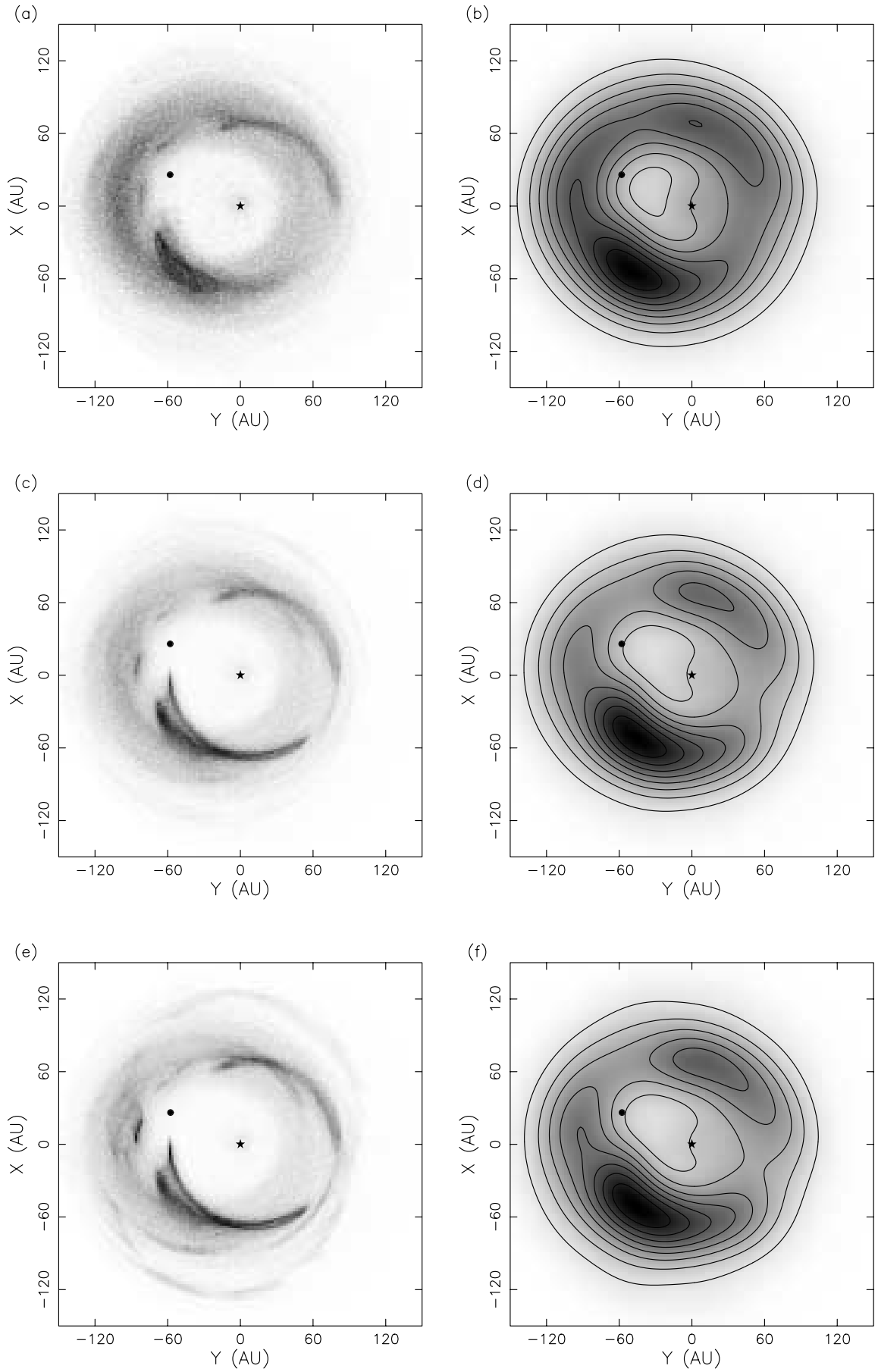

FIG. 6.—Integrated dust distribution from a system containing a Jupiter-mass planet with an eccentricity of 0.5 and a semimajor axis of 44.8 AU, and 500 test particles with $\beta = 0.1$. Parent bodies had initial orbital elements $1.4 < a_{pb}/a_{pl} < 2.0$, $0.0 < e_{pb} < 0.2$, and $0.^{\circ}0 < i_{pb} < 8.^{\circ}0$. Simulated observations used a two-dimensional Gaussian with a FWHM of 40 AU. Plots (*a*) and (*b*) show the dust distribution and a simulated observation after 11.7 Myr (10% of particles remaining). Plots (*c*) and (*d*) show the distribution and a simulated observation after 40 Myr (2% of particles remaining). Plots (*e*) and (*f*) show the distribution and a simulated observation after 153 Myr (no particles remaining). [*See the electronic edition of the Journal for a color version of this figure*.]

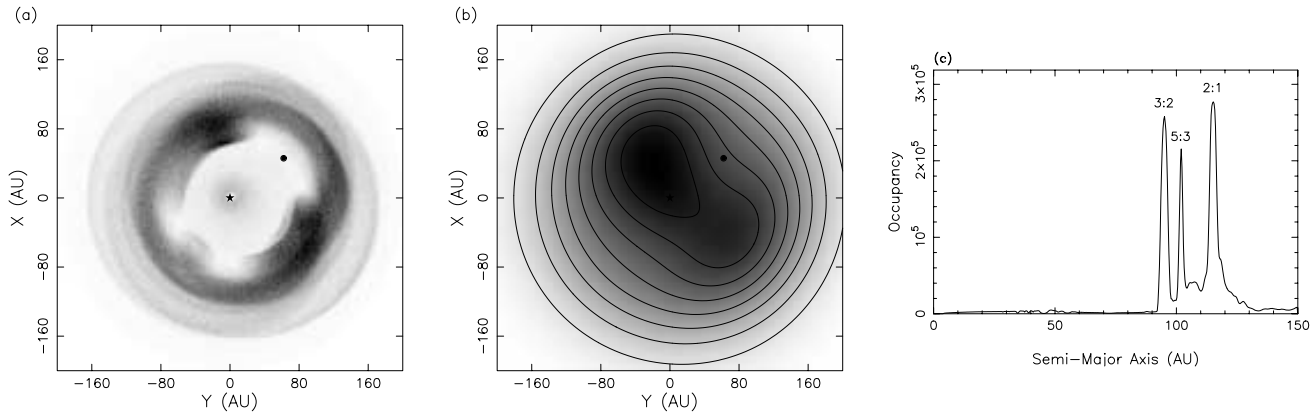

FIG. 7.—Results of Vega simulation using $a_{pl} = 73.7$ AU, $e_{pl} = 0.1$, and 5000 test particles with $\beta = 0.05$ released from parent bodies with 90 AU $< a_{pb} <$ 120 AU, $0.0 < e_{pb} < 0.3$, and $0^\circ < i_{pb} < 8^\circ$. The simulation was terminated after 10^8 yr with 0.6% of particles remaining. (*a*) Dust distribution. Note the two peaks, as seen in the Wilner et al. (2002) interferometric observations. (*b*) Simulated observation of the system using a resolution of 108 AU (equal to the resolution of the 850 μm SCUBA observations by Holland et al. [1998]) and a 5 mJy solar flux, with contours at 2 mJy separation. The two peaks merge together at low resolution, although one dominates slightly. (*c*) Resonance occupancy in the Vega model. [*See the electronic edition of the Journal for a color version of this figure*.]

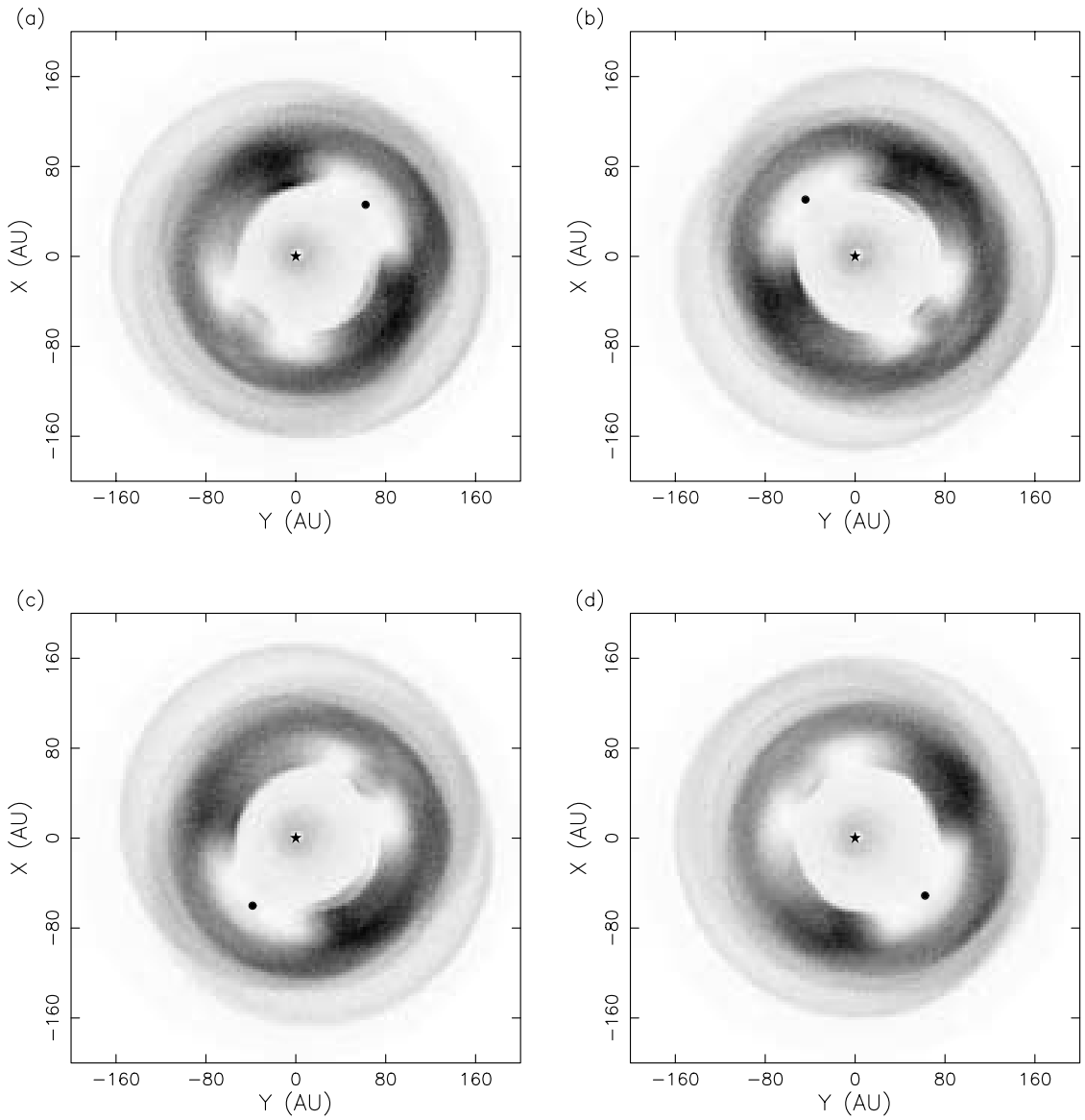

FIG. 8.—Dust distribution generated by the Vega simulations (with $\beta = 0.05$) at the four different recorded planetary phases. The distribution rotates with the planet, meaning that observations from Earth show positional changes in the emission peaks over the planetary period. [*See the electronic edition of the Journal for a color version of this figure*.]

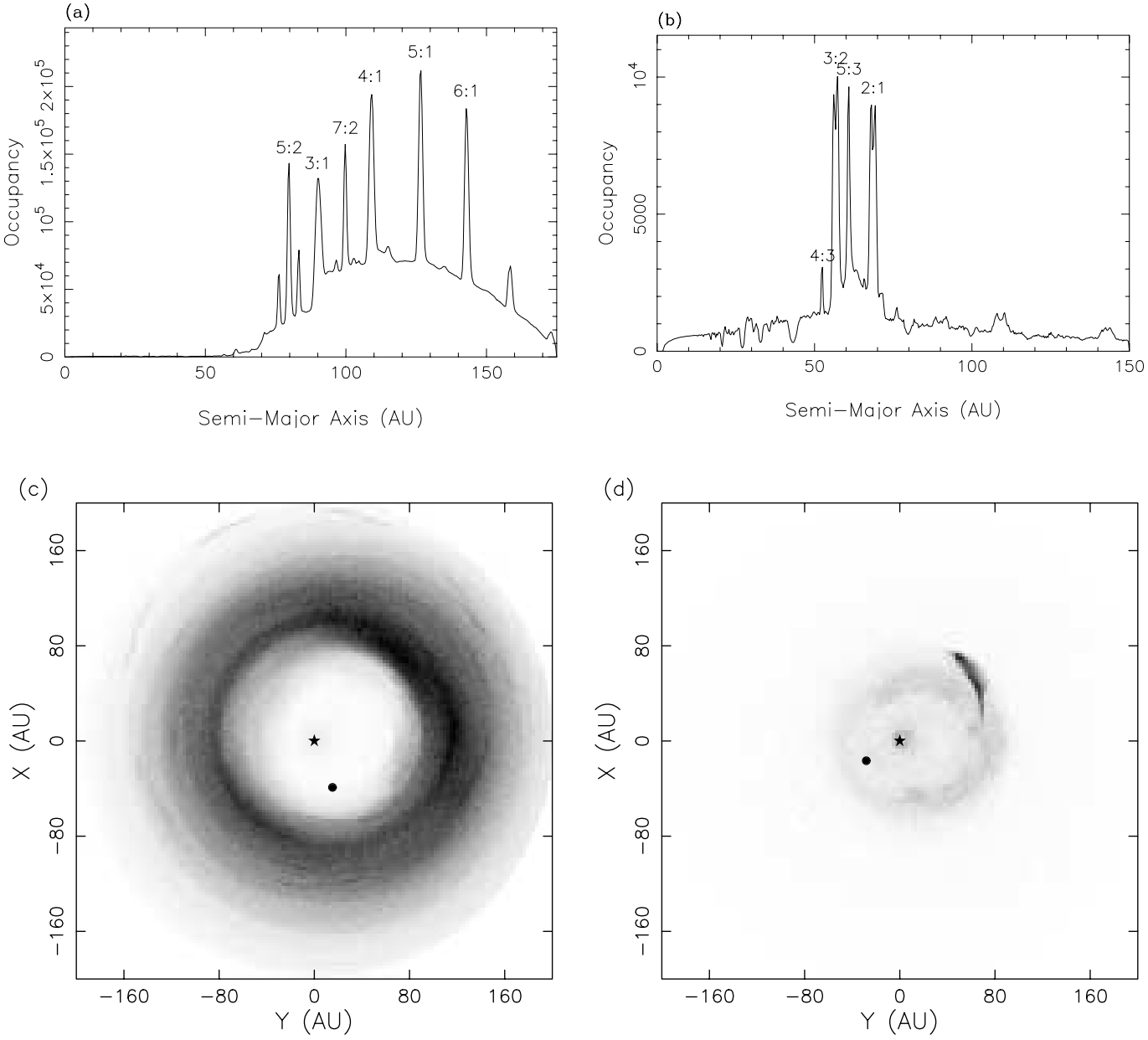

FIG. 9.—Structures resulting from a Jupiter-mass planet with $a_{pl} \sim 44.8$ AU and $e_{pl} = 0.3$. Test particles have $\beta = 0.1$ and are released from parent bodies with initial eccentricity range $e_{pb} = [0.0,\ 0.2]$. (*a*) Resonance occupancy when the initial range of a_{pb} is $[2.0, 3.5]a_{pl}$. The higher order n:1 resonances dominate. Note the high number of total particle positions recorded, indicating longer average particle lifetimes. (*b*) Resonance occupancy when the initial range of a_{pb} is $[1.0, 1.4]a_{pl}$. The planet rapidly removes test particles, and only a few resonances close to the planet's semimajor axis are populated. (*c*) Dust distribution created when the initial range for a_{pb} is $[2.0, 3.5]a_{pl}$. A distinct ring structure is formed, containing two (unequal) density enhancements. (*d*) Dust distribution created when the initial range for a_{pb} is $[1.0, 1.4]a_{pl}$. A ring structure is not generated. [*See the electronic edition of the Journal for a color version of this figure.*]

Plots of occupancy versus semimajor axis are shown in Figure 12 for our preferred model of ϵ Eri (Fig. 12*a*) and models including the addition of a second, Jupiter-mass planet with $e_{pl} = 0.3$ at three different semimajor axes: $a_{pl} = 10$, 15, and 18 AU (Figs. 12*b*, 12*c*, and 12*d*). We see that the addition of a Jupiter-mass planet with a semimajor axis between 10 and 18 AU is capable of substantially reducing particle occupation of semimajor axes less than that of the exterior planet. We found that a planet located too far from the star ($a_{pl} \geq 20$ AU) disrupted the orbit of the outer planet and resulted in a dynamically unstable system. Note the change in the scaling of the graphs in Figure 12. We can clearly see that when an inner planet is included, the resonance occupancy decreases, reflecting a reduction in particle lifetimes. An understanding of the exact effects of a massive inner planet will have to await detailed simulations with large particle numbers, which can resolve the disk at all times. Such an investigation is planned for a future paper.

5.3. *Fomalhaut*

Unlike the previous systems, Fomalhaut has not yet been the subject of detailed numerical simulations. The Fomalhaut system also differs markedly in that 850 μm SCUBA observations suggest that the system is seen nearly edge-on and consists of a dusty torus, rather than a thin disk (Holland et al. 1998). The improved spatial resolution offered by the 450 μm SCUBA images of Holland et al. (2003) confirms the torus structure, while revealing a previously unseen arc of emission near or

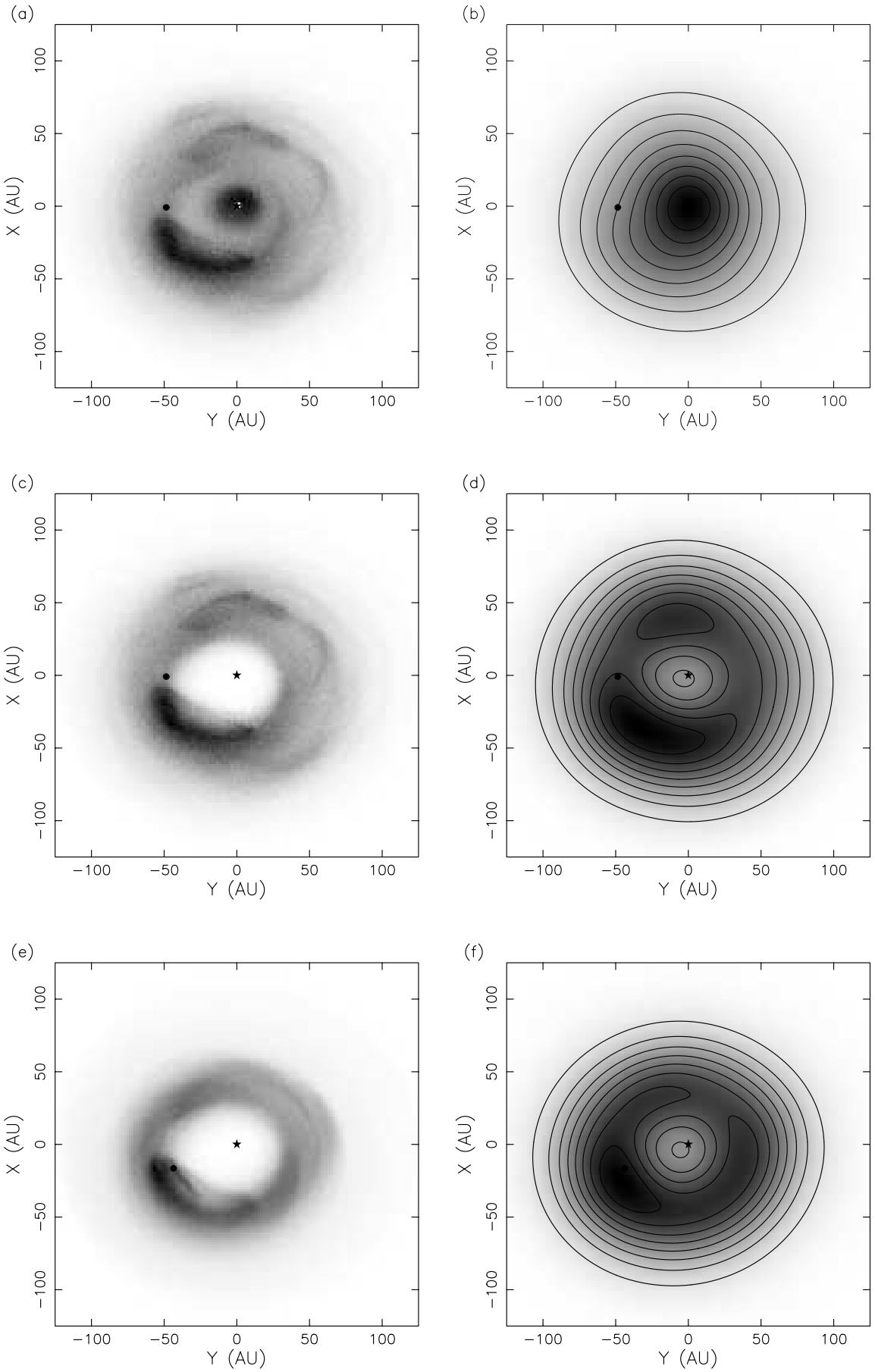

FIG. 10.—Simulations of ϵ Eri including a $M_{\rm pl} = 0.1 M_J$, $e_{\rm pl} = 0.3$ planet with a semimajor axis of 41.6 AU, from a viewing angle of 30°. Parent bodies had $1.1 < a_{\rm pb}/a_{\rm pl} < 1.5$, $0 < e_{\rm pb} < 0.3$, and $0^\circ < i_{\rm pb} < 8^\circ$. The telescope beam FWHM was set to 45 AU, the approximate beam diameter of the Greaves et al. (1998) images. (*a*) Dust distribution, $\beta = 0.1$, with all particles allowed. (*b*) Simulated observation, $\beta = 0.1$, with all particles allowed. Emission close to the star dominates and the ring structure is faint. (*c*) Dust distribution, $\beta = 0.1$, with particles with semimajor axes less than the planet removed. (*d*) Simulated observation, $\beta = 0.1$, with particles with semimajor axes less than the planet removed. (*e*) Dust distribution, $\beta = 0.01$, with particles with semimajor axes less than the planet removed. (*f*) Simulated observation, $\beta = 0.01$, with particles with semimajor axes less than the planet removed. [*See the electronic edition of the Journal for a color version of this figure.*]

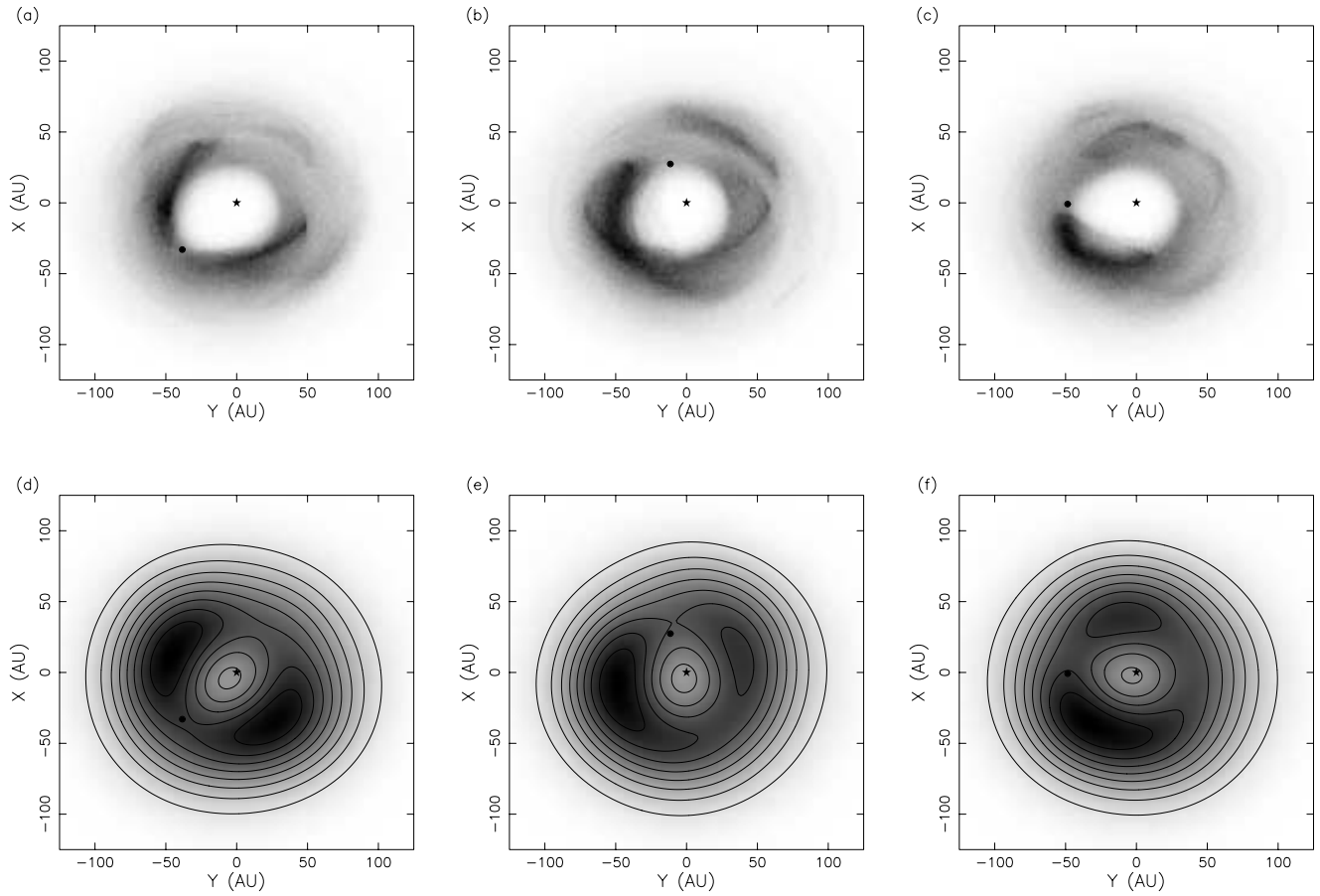

FIG. 11.—Dust distribution and synthetic observations from the ϵ Eri simulations (with $\beta = 0.1$ and particles with semimajor axes interior to the planet removed) at three different planetary phases. Dust distributions are shown in (*a–c*), with the corresponding synthetic observations shown in (*d–f*). The distribution does not rotate with the planet, but the emission peaks show positional changes over the course of an orbit. [*See the electronic edition of the Journal for a color version of this figure*.]

within the torus. This departure from a uniform structure is strongly suggestive of a planetary presence.

The generation of a single arc of emission can be achieved by a 1:1 resonance, as suggested by Holland et al. (2003). Inspection of results for resonance occupancy obtained in the construction of our synthetic catalog, however, indicate that the 1:1 resonance is difficult to populate under normal circumstances. An example is shown in Figure 13, in which a Jupiter-mass planet populates the 1:1 resonance when parent bodies exist interior to the planet, but does not populate the 1:1 resonance when the parent bodies are all external to the planet. We consider it unlikely that parent bodies with semimajor axes slightly less than the planet's semimajor axis would survive for the required length of time. As an alternative explanation of the single arc feature, we find that systems including a massive ($M_{\rm pl} \geq M_{\rm J}$), moderately eccentric ($0.3 \leq e_{\rm pl} \leq 0.5$) planet can induce a single emission arc over a background ring by trapping many particles in the n:1 resonances, where $n > 1$.

After examining our synthetic catalog, we chose a model with the following parameters: $M_* = 2.3\ M_\odot$ (appropriate for an A3 V star such as Fomalhaut; Barrado y Navascues et al. 1997), $M_{\rm pl} = 2M_{\rm J}$, $e_{\rm pl} = 0.4$, and $a_{\rm pl} \sim 59$ AU. Parent bodies were distributed with initial orbital parameters in the following ranges: $0 < e_{\rm pb} < 0.3$, 100 AU $< a_{\rm pb} <$ 180 AU, and $0^\circ < i_{\rm pb} < 25^\circ$. The higher parent body inclinations naturally generate a torus structure, which is believed to exist in the Fomalhaut system. The simulation used 1000 test particles with $\beta = 0.05$, since the mass of dust grains in the Fomalhaut system with diameters >100 μm (corresponding to values of $\beta > 0.1$) is believed to be negligible (Dent et al. 2000). The results of our simulations, which ran until no particles remained after 212 Myr, are shown in Figure 14. The simulated observations bear a close resemblance to the raw 450 μm image of Fomalhaut presented in Holland et al. (2003).

This planetary configuration does generate a dust distribution that does not rotate with the planet but appears fixed from a viewpoint external to the system over an orbital period. Thus, observations of Fomalhaut over time would show no change in emission if this model is correct. The effects of planetary phase are shown in Figure 15.

Although the planetary configuration that we have presented here displays a close similarity to the observations of Fomalhaut to date, as noted above results from our synthetic catalog suggest that several parameters from the model may be varied slightly while still producing similar results. The semimajor axis of the planet is well constrained by the location of the dust ring, but the production of a single arc of emission is seen with several combinations of massive, moderate-eccentricity planets. Thus, this model is only representative of a class of planetary configurations that could be responsible for the structure seen in the Fomalhaut disk.

6. CONCLUSIONS

We have modified an *N*-body symplectic integrator to include the effects of Poynting-Robertson and solar wind drag in order to model collisionless debris disks, and we used the modified

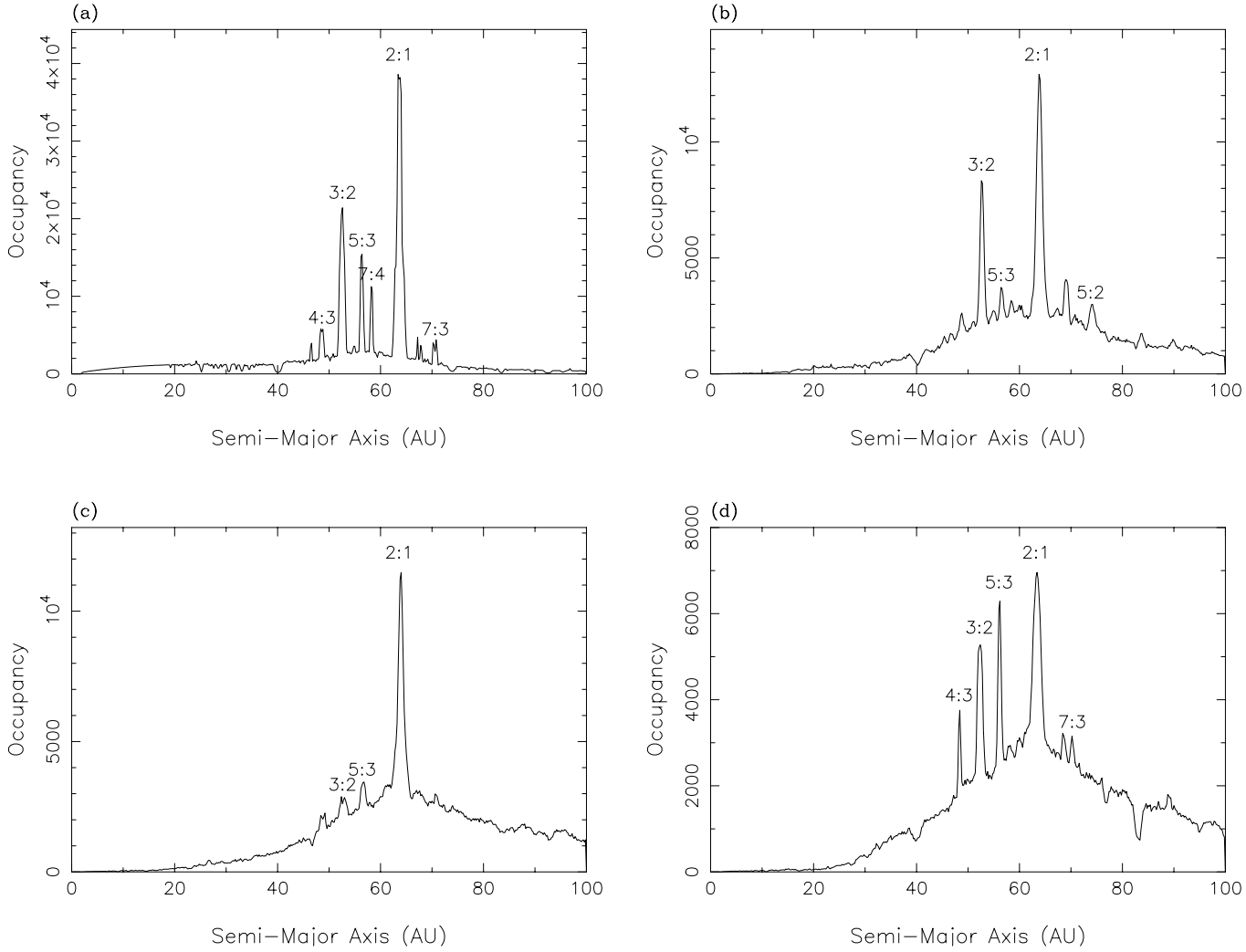

FIG. 12.—Occupancy vs. semimajor axis plots showing the effect of adding a Jupiter-mass, $e_{\rm pl} = 0.3$ inner planet to the ϵ Eri model. Plot (*a*) shows the unmodified ϵ Eri model; note test particle occupancy of semimajor axes interior to 40 AU. Plots (*b*), (*c*), and (*d*) show the results for systems with an inner planet added with a semimajor axis of 10, 15, and 18 AU, respectively. In each case, test particle occupancy of semimajor axes interior to 40 AU is substantially reduced (note the different scales on the four graphs). Simulations contained 500 $\beta = 0.1$ test particles that were released from parent bodies with 46 AU $< a_{\rm pb} <$ 62 AU, $0.0 < e_{\rm pb} < 0.4$, and $0\overset{\circ}{.}0 < i_{\rm pb} < 8\overset{\circ}{.}0$ and were terminated after 10^8 yr.

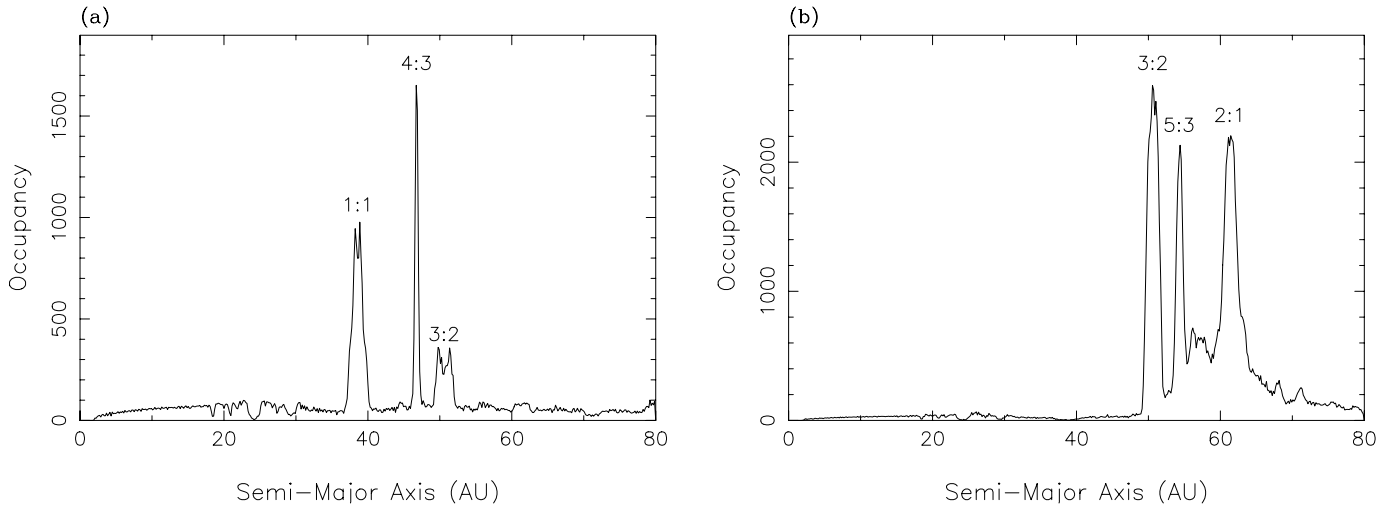

FIG. 13.—Resonance occupancy for a 500 particle simulation of a system containing a Jupiter-mass planet with $a_{\rm pl} = 40$ AU and $e_{\rm pl} = 0.1$. Test particles had $\beta = 0.1$. (*a*) Parent bodies in the ranges 35 AU $< a_{\rm pb} <$ 45 AU, $0.0 < e_{\rm pb} < 0.3$, and $0\overset{\circ}{.}0 < i_{\rm pb} < 8\overset{\circ}{.}0$. The 1:1 resonance is prominent. (*b*) Parent bodies in the ranges 45 AU $< a_{\rm pb} <$ 60 AU, $0.0 < e_{\rm pb} < 0.3$, and $0\overset{\circ}{.}0 < i_{\rm pb} < 8\overset{\circ}{.}0$. There is no population of the 1:1 resonance.

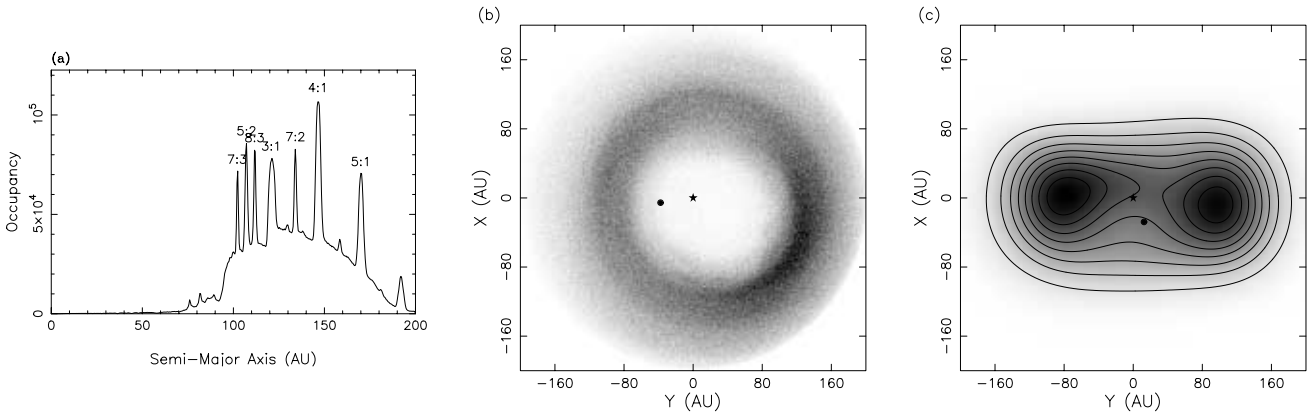

FIG. 14.—Simulations of the Fomalhaut system using a $2M_J$ planet with $e_{pl} = 0.4$ and $a_{pl} \sim 59$ AU. (*a*) Resonance occupation. Note that the n:1 resonances dominate. (*b*) Face-on distribution of particles. (*c*) Simulated observation of system at 450 μm from an inclination of 70°. The telescope FWHM is 50 AU, equivalent to the resolution of SCUBA at 450 μm. Contours show equal-intensity increments. [*See the electronic edition of the Journal for a color version of this figure*.]

integrator to produce a synthetic disk catalog containing approximately 300 model disks. The catalog has two applications: to compare theoretical predictions of disk structure to numerical results and to give an idea of the parameter space that might satisfy a particular observed system, possibly identifying planets that are presently undetectable through Doppler shift techniques. Using this synthetic catalog as a guide, we have produced "best-fit" models for three observed debris disk systems whose disk structures can be explained by the presence of a planetary companion or companions.

We have modeled Vega using a planet with $M_{pl} = 3M_J$, $a_{pl} = 73.7$ AU, and $e_{pl} = 0.1$. The dust distribution generated by this model rotates with the planet, meaning that future observations of Vega should show changes in spatial dust emission as the planetary phase changes. However, since a range of planetary parameters can produce the dust distribution inferred for the Vega system, our solution is representative of that produced by a class of massive ($M_{pl} > M_J$), low-eccentricity ($e_{pl} < 0.2$) planetary companions.

ϵ Eri was modeled using a planet with $M_{pl} = 0.1M_J$, $a_{pl} = 41.6$ AU, and $e_{pl} = 0.3$, a model first proposed by Quillen & Thorndike (2002). Although the dust distribution generated by this model does not rotate with the planet, it does change over the course of an orbital period, offering hope for confirmation by future observations. However, this model is dependent on the existence of a second, massive inner planet to clear particles interior to the modeled planet, which cannot be simulated using the techniques outlined in this paper.

We modeled Fomalhaut using a planet with $M_{pl} = 2M_J$, $a_{pl} = 59$ AU, and $e_{pl} = 0.4$. The dust distribution generated by this model does not change significantly over the course of a planetary orbit, and thus the effect of planetary phase would be difficult to detect in future observations. Like the model presented for Vega, our model for Fomalhaut is the best match to current observations from a class of massive, moderate-eccentricity planets that generate similar structure.

Numerical modeling of planets in dusty debris disks has shown that planets that are undetectable through present techniques are likely to be responsible for the observed asymmetries of known debris disk systems. It should be noted, however, that it is difficult to positively identify a unique planetary companion without temporal information showing the changes in disk structure over the course of a planetary orbit.

The authors wish to thank Hal Levison for useful discussions about RMVS3 and Dave Wilner for providing an unpublished 350 μm ϵ Eri image. We also thank the anonymous referee for providing useful feedback and suggestions. A. D. was supported by a Summer Vacation Scholarship from the Swinburne Centre for Astrophysics and Supercomputing. All simulations were run on the Swinburne supercomputer.[2]

Our synthetic debris disk catalog is available online at http://astronomy.swin.edu.au/debrisdisks.

[2] See http://supercomputing.swin.edu.au.

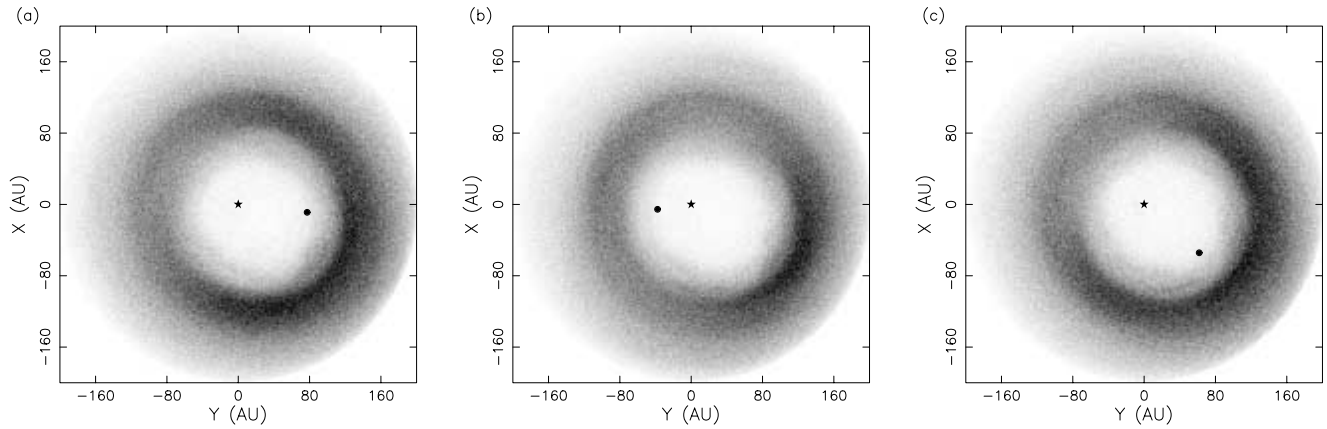

FIG. 15.—Dust distribution generated by the Fomalhaut simulations at three different planetary phases. The distribution does not rotate with the planet and remains relatively constant in a fixed reference frame. [*See the electronic edition of the Journal for a color version of this figure*.]

REFERENCES

Aumann, H. H. 1985, PASP, 97, 885
Aumann, H. H., et al. 1984, ApJ, 278, L23
Backman, D. E., Dasgupta, A., & Stencel, R. E. 1995, ApJ, 450, L35
Backman, D. E., & Paresce, F. 1993, in Protostars and Planets III, ed. E. H. Levy & J. I. Lunine (Tucson: Univ. Arizona Press), 1253
Barrado y Navascues, D., Stauffer, J. R., Hartmann, L., & Balachandran, S. C. 1997, ApJ, 475, 313
Burns, J. A., Lamy, P. L., & Soter, S. 1979, Icarus, 40, 1
Clampin, M., et al. 2003, AJ, 126, 385
Dent, W. R. F., Walker, H. J., Holland, W. S., & Greaves, J. S. 2000, MNRAS, 314, 702
Dermott, S. F., Jayamaran, S., Xu, Y. L., Gustafson, B. A. S., & Liou, J.-C. 1994, Nature, 369, 719
Duncan, M. J., Levison, H. F., & Lee, M. H. 1998, AJ, 116, 2067
Greaves, J. S., et al. 1998, ApJ, 506, L133
Hatzes, A. P., et al. 2000, ApJ, 544, L145
Holland, W. S., et al. 1998, Nature, 392, 788
Holland, W. S., et al. 2003, ApJ, 582, 1141
Kuchner, M. J., & Holman, M. J. 2003, ApJ, 588, 1110
Landgraf, M., Liou, J.-C., Zook, H. A., & Grün, E. 2002, AJ, 123, 2857
Levison, H. F., & Duncan, M. J. 1994, Icarus, 108, 18
Liou, J.-C., & Zook, H. A. 1997, Icarus, 128, 354
———. 1999, AJ, 118, 580
Liseau, R. 1999, A&A, 348, 133
Moro-Martin, A., & Malhotra, R. 2002, AJ, 124, 2305
Ozernoy, L. M., Gorkavyi, N. N., Mather, J. C., & Taidakova, T. A. 2000, ApJ, 537, L147
Quillen, A. C., & Thorndike, S. 2002, ApJ, 578, L149
Wilner, D. J., Holman, M. J., Kuchner, M. J., & Ho, P. T. P. 2002, ApJ, 569, L115
Wisdom, J., & Holman, M. 1991, AJ, 102, 1528
Wyatt, M. C., & Dent, W. R. F. 2002, MNRAS, 334, 589
Wyatt, S. P., & Whipple, F. L. 1950, ApJ, 111, 134
Zuckerman, B. 2001, ARA&A, 39, 549